REPORT DOCUMENTATION PAGE			Form Approved OMB No. 0704-0188

Public reporting burden for this collection of information is estimated to average 1 hour per response, including the time for reviewing instructions, searching existing data sources, gathering and maintaining the data needed, and completing and reviewing the collection of information. Send comments regarding this burden estimate or any other aspect of this collection of information, including suggestions for reducing this burden, to Washington Headquarters Services, Directorate for Information Operations and Reports, 1215 Jefferson Davis Highway, Suite 1204, Arlington, VA 22202-4302, and to the Office of Management and Budget, Paperwork Reduction Project (0704-0188), Washington, DC 20503.

1. AGENCY USE ONLY *(Leave blank)*	2. REPORT DATE	3. REPORT TYPE AND DATES COVERED
	1.Jul.99	MAJOR REPORT

4. TITLE AND SUBTITLE
GROUND-BASED INTERCEPT OF A BALLISTIC MISSILE INFRARED SENSOR DESIGN

5. FUNDING NUMBERS

6. AUTHOR(S)
2D LT DEYOUNG DANIEL S

7. PERFORMING ORGANIZATION NAME(S) AND ADDRESS(ES)
UNIVERSITY OF COLORADO AT COLORADO SPRINGS

8. PERFORMING ORGANIZATION REPORT NUMBER

9. SPONSORING/MONITORING AGENCY NAME(S) AND ADDRESS(ES)
THE DEPARTMENT OF THE AIR FORCE
AFIT/CIA, BLDG 125
2950 P STREET
WPAFB OH 45433

10. SPONSORING/MONITORING AGENCY REPORT NUMBER
FY99-172

11. SUPPLEMENTARY NOTES

12a. DISTRIBUTION AVAILABILITY STATEMENT
Unlimited distribution
In Accordance With AFI 35-205/AFIT Sup 1

12b. DISTRIBUTION CODE

13. ABSTRACT *(Maximum 200 words)*

DISTRIBUTION STATEMENT A
Approved for Public Release
Distribution Unlimited

14. SUBJECT TERMS	15. NUMBER OF PAGES
	24
	16. PRICE CODE

17. SECURITY CLASSIFICATION OF REPORT	18. SECURITY CLASSIFICATION OF THIS PAGE	19. SECURITY CLASSIFICATION OF ABSTRACT	20. LIMITATION OF ABSTRACT

GROUND-BASED INTERCEPT OF A BALLISTIC MISSILE

INFRARED SENSOR DESIGN

by

DANIEL SPENCER DeYOUNG

B.S., UNITED STATES AIR FORCE ACADEMY, 1998

A creative investigation submitted to the

Graduate Faculty of the

University of Colorado at Colorado Springs

in partial fulfillment of the

requirements for the degree of

Master of Engineering

Department of Mechanical and Aerospace Engineering

1999

DTIC QUALITY INSPECTED 2

19990804 201

© Copyright By Daniel Spencer DeYoung

All Rights Reserved

DeYoung, Daniel Spencer (M.E., Space Operations)

Ground-Based Intercept of a Ballistic Missile: Infrared Sensor Design

Creative investigation directed by Doctor Don Caughlin

This investigation encompasses a study of the operation of infrared detectors and applies this knowledge to the design of a space-based infrared sensor. The design process is illustrated, and sensor technology is explored in order to provide design options at each step. The infrared sensor system designed in this investigation is a component of a ballistic missile defense simulation and is required to sense a ballistic missile threat during the launch and boost phases. The product of this study is a point design that will, with iterative runs of the working simulation, be refined to achieve maximum utility in the integrated architecture. Continual analysis provided as the design matures explains the limits and merits of the system.

CONTENTS

TABLES

Table

FIGURES

Figure

I. INTRODUCTION

PURPOSE AND SCOPE OF STUDY

The space-based infrared detection system is the component of the ground-based interceptor missile defense system that first senses the incoming threat. A missile in flight radiates in the infrared through its plume, and from its surface due to atmospheric drag and (to a lesser extent) reflected solar and terrestrial radiation. The infrared region of the spectrum is generally defined as the wavelengths from approximately 750 nanometers to 1 millimeter (reference 1, p 3). Though these wavelengths are not visible to the human eye, they do behave like visible light in that they can be focused through optics and detected with photodetectors. This is exactly how the space-based infrared detection system operates. This creative investigation is a study of the physics and technology of infrared detectors, and an application of this information to the design of an infrared sensor for this simulation.

II. THE DESIGN PROCESS

The first step in the design process is to understand the requirements of the sensor. There will always exist functional requirements that delimit and constrain the options available to the designer at each step as the

architecture matures, until finally an initial point design is created. The design process is an iterative one, and the point design matures with each new spiral in the design process. The results presented in this investigation are the product of many iterations of the process, involving tradeoffs among the parameters until a satisfactory sensor was designed.

DETECTOR TYPES

An infrared system can be designed as a detector, tracker, imager, or a combination of the three. It is the requirement of the system that determines which of these functions the infrared sensor must perform. A detector design is sufficient for determining the presence of a source of radiation within its field of view. The wavelengths which can be detected, and the total amount of radiation that must be collected before detection can occur are functions of the detector design. A tracker is a detector that is configured such that it can continually relocate its field of view to follow a moving source, and report the target's track to some other entity. Tracking usually involves a smaller field of view than a detector in search mode in order to achieve better spatial resolution, and therefore better accuracy. An imager is able to use infrared radiation as a camera uses visible light,

collecting and processing it to form an image. Although imagers can be used for detection and tracking purposes, their most common use is to provide a visual representation of surroundings for human interpretation. An example of such a system is the forward-looking infrared system developed by the military to provide pilots with environmental information in low-light situations (reference 3, p 212).

The infrared sensor that is required for this simulation could be either a detector or a tracker. Since the battle manager only needs to determine one position from the infrared sensor information, a detector would be a sufficient design. A tracking sensor is desirable, however. It can aid in identifying false alarms, provide additional position information if the tracking radar loses the target, and give a measure of redundancy to the system by providing a backup (albeit less accurate) track capability.

SOURCE RADIATION

Before any variety of sensor can be built, the engineer must have an understanding of the target to be sensed. With this information, the radiation source can be modeled, and the appropriate sensor components can be chosen accordingly. The infrared sensor for this

simulation has to detect a launching ICBM, and so the plume energy must be detected. In addition, atmospheric heating quickly becomes a factor as the ICBM accelerates. These two factors combine to form the radiation source.

The primary figure of merit for the sensor will be its signal-to-noise ratio (S/N), which has as input the incident radiation flux. The flux can be determined by assuming the source to be a blackbody and using the Stefan-Boltzmann law, but the temperature of the source must first be known.

All electromagnetic radiation is characterized by the family of blackbody curves, which at a given temperature relate the intensity of emitted radiation to the wavelength emitted. Each curve is a function given by Planck's Radiation Law (Equation 1), plotted in Figure 1.

$$E(\lambda, T) := \frac{2 \cdot \pi \cdot h \cdot c^2}{\lambda^5} \cdot \left(\frac{1}{e^{\frac{c \cdot h}{k \cdot T \cdot \lambda}} - 1} \right) \qquad (1)$$

where

h= 6.626076 E-34 J s, Planck's constant

c= 2.997925 E8 m/s, speed of light

λ= wavelength m/s

k= 1.380658 E-23 J/K, Boltzmann constant

T= temperature, K

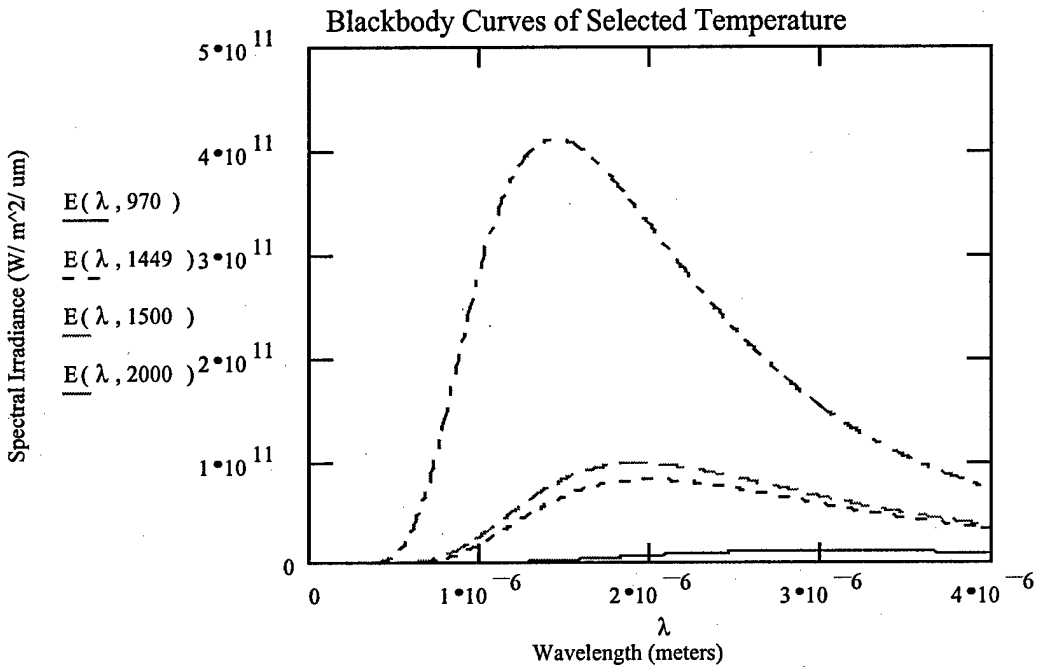

Figure 1

In order to estimate the temperature of the missile plume and plot its blackbody curve, we applied reverse engineering. Starting with the fact that the band of "wavelengths between 1 and 3 micrometers…is used by space-based sensors to see the bright rocket plumes of boosting missiles" (reference 7, p 4), we applied Wien's Displacement Law (Equation 2) to find an approximate temperature for the plume.

Wien's Displacement Law is found by taking the derivative of Equation 1, and setting it equal to zero. The equation is shown below, and 2 microns was chosen as the representative wavelength for plume detection; this

choice assumes that the range quoted above is designed to detect the wavelengths of maximum energy radiation that transmit well through Earth's atmosphere:

$$T := \frac{2.897756 \cdot 10^{-3}}{\lambda_{plume}} \qquad T = 1.449 \cdot 10^{3} \quad \text{Kelvin} \qquad (2)$$

The blackbody curve for this temperature is among those plotted in Figure 1. Finally, the total power emitted by a blackbody at the temperature of the rocket plume is given by the Stefan-Boltzmann Law, which calculates the area under the curve. The Stefan-Boltzmann Law is found by integrating Equation 1 over all wavelengths, and yields the total radiant emittance, shown below:

$$W_b := \sigma \cdot T^4 \qquad W_b = 2.5 \cdot 10^{5} \quad W\,m^{-2} \qquad (3)$$

where

T= 1449 K, missile plume temperature

σ= 5.66051 E-8 W m^{-2} K^{-4}, Stefan-Boltzmann constant

Next, the size and shape of the plume were estimated. Plume size varies with altitude, becoming very large at high altitudes. A system requirement for this sensor is to detect the ICBM as it launches, however, so we approximated the plume as a relatively small sphere of radius 3 meters. Thus, the total power emitted by the ICBM plume was found

by simply multiplying the total radiant emittance given by the surface area of the plume-sphere, yielding a value of:

$$W_b \cdot \left(4 \cdot \pi \cdot r_{plume}^{\ 2}\right) = 2.827 \cdot 10^7 \quad \text{Watts}$$

To complete the radiation source model, we repeated the above process and found the contribution of aerodynamic heating. From a graph of measured skin temperatures vs. Mach number we estimated the missile's temperature to be 970 K (reference 3, p 230). The Mach number came from a computer model that describes a Titan missile launch. After the first stage burnout (125 seconds after launch) the Mach number is equal to approximately 4.62. Again, the Stefan-Boltzmann Law gives the total radiant emittance from the missile skin. Dimensions listed in reference 11 (p 267) were used to calculate the surface area. The total radiant emittance and total power emitted due to aerodynamic heating are:

$$W_b = 5.02 \cdot 10^4 \quad W\ m^{-2}$$

$$\text{Power} = 6.337 \cdot 10^7 \quad \text{Watts}$$

It is perhaps surprising that the aerodynamic heating radiates more power than does the missile plume radiation, albeit using Mach numbers estimated at the first stage burnout. In addition, the peak wavelength of a blackbody

that radiates at 970 Kelvin is again given by Equation 2, and is equal to 2.987 μm.

ORBIT DETERMINATION

The flux received at the detector is now a function of atmospheric attenuation and the detector's altitude. The altitude is determined by the orbit, which in turn is influenced by the requirements of the sensor. The lower the orbit, the better the detector is able to spatially resolve objects. Yet a geostationary orbit removes the complexity of a satellite's motion relative to the Earth, and maximizes the ground area a single detector can cover at any one time. If the infrared system were required to provide commit-quality tracking and target discrimination capabilities, a low orbit and all its complexities would be imperative. However, this system needs only provide the general location of a possible threat--one that is sufficiently accurate that ground-based radar can locate the threat and identify it as such. Therefore, the geostationary orbit was the better design choice for this simulation, trading an acceptable loss in resolution for the simplicity of the orbit.

ATMOSPHERIC ATTENUATION

Atmospheric attenuation is a much more difficult parameter to predict. The optical properties of the

atmosphere are, as for most optical elements, a function of wavelength. A rigorous analysis with a high-fidelity atmospheric model might adequately reflect how the atmosphere acts on the radiation source components in different ways. Since such high-fidelity models are few in number and extremely expensive to come by, a far less-rigorous model was applied.

There are three main atmospheric windows in the infrared portion of the spectrum. One begins in the visible wavelengths and terminates near 2 microns in the short-wave infrared region (SWIR). The second covers 3 to 5 microns in the middle-wave region (MWIR), and the third spans 8 to 14 microns in the long-wave region (LWIR) (reference 1, p 33). Attenuation still occurs to a varying degree within each window, but is low enough to allow for detection of ground objects from space. Attenuation occurs because certain gas constituents of air are excited by the propagating frequencies. The atmosphere is in a constant state of flux, its relative mix of constituents and its overall altitude changing with time of day and time of year. A graph approximating transmission (%) versus wavelength is included as Figure 2. For this simulation the transmission percentage for the plume was taken at

Atmospheric Transmissions vs. Wavelength

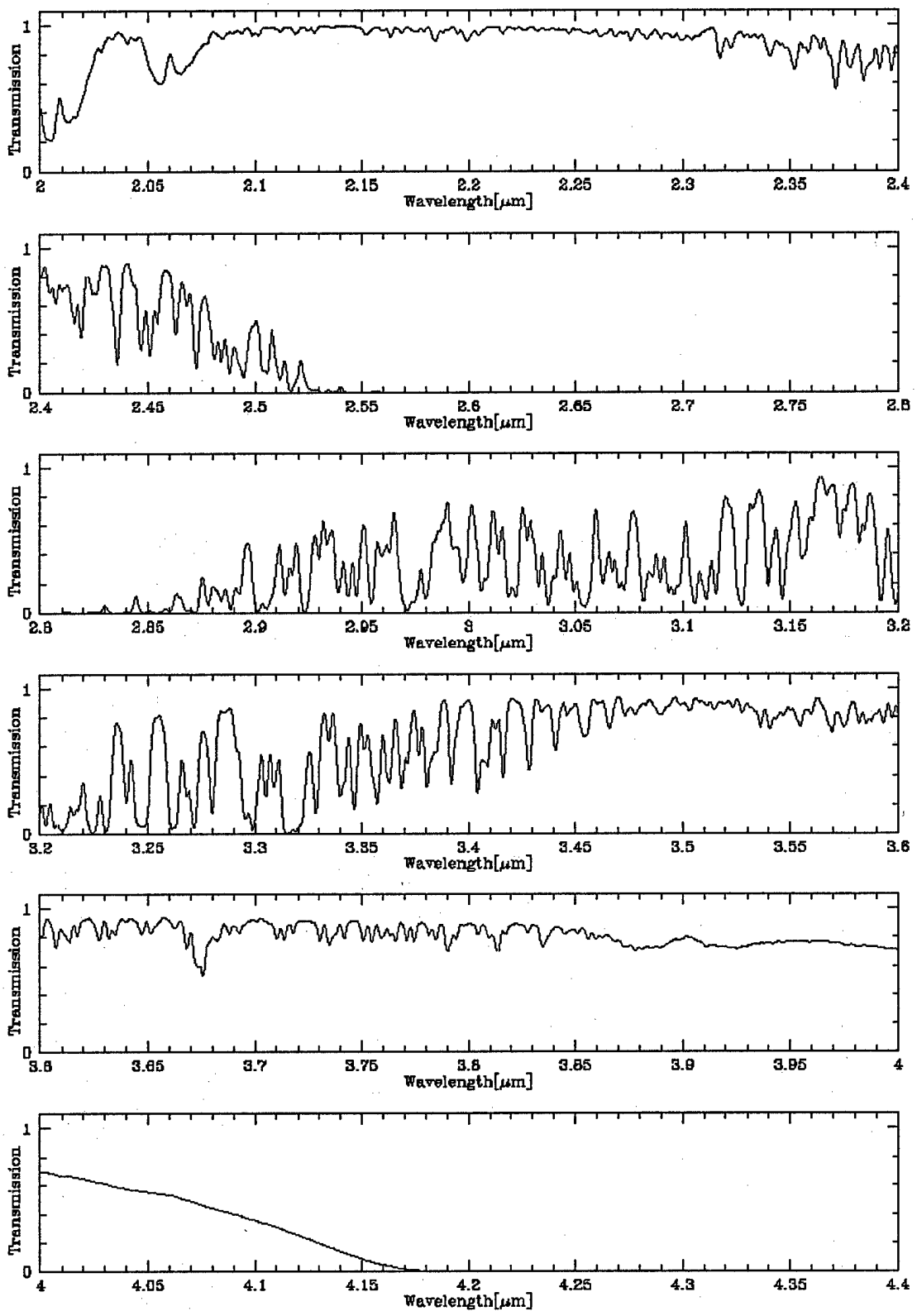

Figure 2, (reference 12)

2.2 microns, a window close to the plume radiation's peak wavelength, and was found to be approximately 80%. For the atmospheric heating radiation, Figure 2 yielded an approximate 40% transmission value.

ARRAY MATERIAL AND SIZING

The flux at the sensor is now calculable, but the amount of radiation flux the sensor can collect is a function of the lens size. Yet lens size is dually constrained. Not only must it be large enough to allow sufficient radiation through to achieve a high S/N, but it must also be sized to perform the focusing required of it. The system requirements combined with our choice of orbit to guide the initial lens and sensor configuration.

The design process does not always flow neatly from step to step. Before continuing to calculate the lens size, it is necessary to first discuss the design of the detector array and its "optical-detection process" (reference 1, p 86). The optical-detection process describes specifically how the incident radiation (photons, if using the quantum model) interact with the detector material to register a signal. The selection of a process type will determine the array size and capabilities, which in turn will affect the lens design.

Optical-detection processes can employ a photon-detection mechanism or a thermal detection mechanism. The latter is generally less timely and efficient than the former, and will therefore not be discussed.

The photon-detection mechanism is accomplished in one of three ways: by photovoltaic detection, photoconductive detection, or photoemissive detection. Photovoltaic detectors operate by converting an incident photon into a current (voltage). Photoconductive detectors, broken into extrinsic and intrinsic varieties, work by converting an incident photon into a change in resistance or conductance of the material. The extrinsic variety is doped with some material designed for detection of the longer infrared wavelengths. For both photovoltaic and photoconductive detectors, the electron produced by the incident photon is excited from the valence to the conduction band of the semi-conductor material, but remains in the array material. A photoemissive detector works by ejecting an electron in response to an incident photon. This electron is then free and travels across a vacuum to be collected at an anode and registered as current. This process is inherently less efficient than the first two (reference 1, p 93-9).

Detector Type	η (%)
Photoconductor (intrinsic)	~60
Photoconductor (extrinsic)	~30
Photovoltaic	~60
Photoemissive	~10
Photographic Film	~1

Table 1

The measure of a detector's quality is termed quantum efficiency, and is a ratio of the number of electrons created by incident photons to the number of incident photons. Table 1 compares typical quantum efficiencies for the different detector types described above (reference 1, p 88).

A photovoltaic HgCdTe detector was chosen for two reasons. First, it was possible to find and compare values for this detector with other types (e.g. a reference to a 65% quantum efficient HgCdTe material designed to detect in or near the wavelengths emitted by the sources (reference 1, p 94)). Second, "most SWIR, MWIR, and LWIR detectors are made of either Mercury-Cadmium-Telluride (HgCdTe), or Indium Antimonide (InSb)" (reference 7, p 5). *Space Mission Analysis and Design* (p 259) gives specifications

for an HgCdTe array, which was chosen as a basis for the sensor.

With the material properties now selected, the array was be sized. Most commercial arrays are 256 X 256 pixels in size or smaller. The point design assumed an array size of 101,787 pixels (array radius of 180 pixels), larger than the 65,536 pixel arrays to somewhat compensate for the resolution disadvantages of a geostationary orbit. A summary of the array material and dimensions is organized in Table 2.

Detector Material	Spectral Response (μm)	Operating Temp (K)	Array Diameter	Pixel Size (μm)	τ (μs)
HgCdTe	3-5	77	720 pixels	100 X 100	.2-.8

Table 2 (adapted from SMAD, p 259)

SENSOR OPTICS

It is now possible to return to the task of sizing the lens. Each pixel in the focal plane array corresponds to an area of the footprint termed the "resolution element". The angular diameter of each resolution element is described by the trigonometric expression,

$$\theta_r := \operatorname{atan}\left(\frac{2 \cdot re_{radius}}{alt_{geo}}\right) \qquad \theta_r = 5.587 \cdot 10^{-5} \quad \text{radians} \qquad (4)$$

where re_{radius} is the resolution element radius, alt_{geo} is the detector's geosynchronous altitude, and the Earth is assumed to be flat under the footprint. Given that the lens must resolve each resolution element and map it onto a single pixel, it can be sized according to the diffraction-limited angular resolution equation, shown below:

$$D := \frac{1.22 \cdot \lambda_{IR}}{\theta_r} \qquad D = 0.065513 \quad \text{meters} \qquad (5)$$

Thus, the final design for the lens was 6.55 cm. As mentioned, lens design is dually constrained. This sizing was the result of iteration to satisfy both resolution requirements and flux-gathering requirements to achieve a sufficient S/N. The next step, then, is to calculate the signal to noise figure of merit. It will show that the model and final design are sufficient.

FIGURES OF MERIT

The signal to noise ratio may be written as:

$$StoN\left(atm_{trans}\right) := \frac{\pi \cdot D \cdot J_t \cdot D_{star} \cdot L}{4 \cdot \left(f_{number}\right) \cdot Range^2} \cdot \left(\frac{n \cdot T_f}{\Omega_s}\right)^{.5} \cdot atm_{trans} \qquad (6)$$

(reference 10, p 280)

There are still a few variables to define before the S/N will yield values. Thus far, the design includes:

$D := .0655$	meters
$J_{t\_plume} := 2.25 \cdot 10^{6}$	Watts/unit solid angle
$J_{t\_skin} := 5.043 \cdot 10^{6}$	Watts/unit solid angle
$D_{star} := 4 \cdot 10^{8}$	m $Hz^{1/2}$ / W
$n := 101787$	number of pixels
$range := alt_{geo}$	meters, will vary as ICBM moves
$atm_{trans\_plume} := .8$	
$atm_{trans\_skin} := .4$	
$\Omega_s = 2.495 \cdot 10^{-4}$	steradians, about footprint

The variables of the S/N equation that are yet to be defined are the loss term (L), the frame time (T_f), and the f/# (f_{number}). Actually, f/# is has already been implicitly defined, since it is the ratio of focal length to lens diameter. The focal length equation and its result are shown below, along with the f/#:

$$f := \frac{r_{array} \cdot h}{fp_{radius}} \quad \text{meters} \qquad (7)$$

$$f = 2.02 \quad \text{meters} \qquad f_{number} = 42.041$$

The focal length is defined above according to simple geometry, where the variables are the radius of the detector (image) array, the height of the detector, and the footprint radius. The resultant f/# was large, and was an unfortunate result of choosing the geostationary orbit. The f/# is a measure of the "speed" of the optic, a smaller value indicating that more radiation can be focused at a

shorter distance. Usually this value is designed to be as close to one as possible, because shorter focal lengths yield smaller focal spot diameters. This in turn means more radiation focused onto each pixel and a higher S/N (reference 1, p 498).

The loss term is comprised of several constituent losses, to include an optics loss, electronics loss, detector loss, scanning factor loss, and a loss-related coefficient termed the "bandwidth proportionality constant" (reference 10, p 180). These losses are, unfortunately, factors determined either experimentally from a constructed system or estimated from a complete system design. While this investigation did not design the detector at that level of detail, it was still important to estimate these loss terms for the S/N estimate to be reasonable. *Introduction to Sensor Systems* reports that each of these loss terms typically ranges from 0.5 to 1.0, except for the bandwidth proportionality constant which can attain values greater than 1. Loss terms were estimated as .7 each, with the bandwidth proportionality constant equal to 1. This yielded an overall transmission factor (distinct from atmospheric attenuation) of 0.287.

The frame time is influenced by the system requirements. The true requirement to drive all others is

that the ground based-interceptor destroys the ICBM exoatmospherically. This requirement flows to the infrared sensor in that the timeliness of detection must be adequate to achieve the exoatmospheric kill. This "floating" time limit is only determinable by thoroughly evaluating the simulation as an integrated system. For the purpose of this S/N calculation, every spot on the pertinent hemisphere of Earth should be covered every 30 seconds. Since there are two sensors on two satellites they can be timed to work in tandem, each covering their hemisphere once every minute. The dwell time of any single detector over a resolution element is therefore given by:

$$t_d := \frac{re_{radius}}{(rot\_rate \cdot R_e)} \qquad t_d = 1.497 \cdot 10^{-4} \quad \text{seconds} \qquad (8)$$

and the frame time can be calculated using the following equation:

$$T_f := t_d \cdot n \qquad T_f = 15.233 \quad \text{seconds} \qquad (9)$$

The S/N due to each source was computed and added together to form a total S/N:

$$StoN_{plume}(atm_{trans}) = 21.23 \qquad StoN_{skin}(atm_{trans}) = 23.791$$

$$StoN_{total} = 45.018 \qquad 10 \cdot \log(StoN_{total}) = 16.534 \quad dB$$

The S/N of the atmospheric heating was higher than the plume S/N. This shows that even though it was modeled with

a lower temperature, it had a much larger surface area through which to radiate, and so produced more power. The total S/N value was next evaluated as to whether it met detection criteria.

How does one know whether a S/N value is sufficient? One final calculation provided the answer. The false alarm rate (FAR) of a detector gives the number of false alarms per time, and is a function of S/N ratio. The system requirements determine whether the FAR is too high, and therefore whether the S/N is too low. False alarms are modeled stochastically, but are actually due to noise radiation.

The semi-conductor materials that comprise the array of detectors operate by having incident photons excite detector electrons into a conduction band. Since infrared radiation has such low energy, the energy gap between the valence and conduction bands is necessarily small. Therefore, relatively small noise radiation (of equal or greater energy to signal radiation) will register and cause a false alarm. This is the reason infrared detectors must be cooled (the array in this design is cooled to 77 K), because even the thermal energy of the detector itself (in the form of phonons, or sound particles moving through the array lattice) can be energetic enough to cause false

alarms. Cooling the array reduces lattice vibrations and the energy of resultant phonons (reference 1, p 91).

The equation that yields false alarm rate is provided below:

$$FAR = \frac{P_n \cdot n}{t_d} \cdot L_{scanning} \qquad (10)$$

P_n is the probability of false alarm. A chart relating S/N, probability of detection, and P_n is presented in *Introduction to Sensor Systems*. The purpose of the ground-based interceptor ballistic missile defense system is to protect against missile attacks, and from this purpose flows yet another requirement for the infrared sensor. The probability of detection had to be designed as close to 100% as possible. Using the aforementioned graph with a value of 99.9% for probability of detection and the calculated S/N of 16.534 dB, the probability of false alarm value was P_n= 10^-10 (reference 10, p 182). Substituting values into Equation 10, the false alarm rate was found to be:

$$FAR = 0.048 \quad \text{false alarms/ second}$$

Over the course of a day, then, each infrared sensor will report 4,147.2 false alarms to the battle manager. This value may seem high, but for this system it is quite acceptable. First of all, there are two satellite sensors,

both of which must transmit data to the battle manager before the search radar is cued to perform its duties. Therefore, both sensors would have to register false alarms over the same region of the field of view. Yet even if the battle manager fed the search radar 4,147 phantom missiles to look for, it would find no threat and report such back to the battle manager. The search radar is the higher-fidelity component in the system, and its powerful (though less timely) detection capabilities are the perfect balance to the infrared false alarms. The final analysis shows that this sensor design is a sufficient one.

III. CONCLUSIONS

This investigation reviewed the design process for an infrared sensor, and explained the physical phenomenon related to infrared detection. The sensor requirements were outlined, and proved to force or influence every aspect of the design. The target was modeled as two separate sources of radiation, each contributing to the final S/N. In fact, it was found that atmospheric heating was a greater source of radiation flux at the detector than was the plume radiation.

Atmospheric attenuation was dealt with in enough detail to estimate values for the design. Then the process by which the incident radiation is converted to a signal

was explained, and an understanding of that process guided the selection of an array material. From there the detector array was sized, followed by the optics. The dwell time was derived from system requirements, and values were estimated for the loss terms in the signal to noise equation. Finally, the signal to noise figure of merit was calculated and converted into a false alarm rate, which is sufficient for this system architecture. Thus, the design process has produced a design. The simulation will now be instrumental in refining the design. Although much iteration was required to arrive at this preliminary design, a thorough assessment of integrated system performance will improve it.

Bibliography

1. Dereniak, E.L. and Boreman, G.D., *Infrared Detectors and Systems*. John Wiley & Sons, Inc., New York, 1996, (pages).
2. Zissis, George J. (ed.), *The Infrared & Electro-Optical Systems Handbook: Volume 1, Sources of Radiation*, Environmental Research Institute of Michigan, Ann Arbor, MI, 1993.
3. Campana, S. B. (ed.), *The Infrared & Electro-Optical Systems Handbook: Volume 5, Passive Electro-Optical Systems*, Environmental Research Institute of Michigan, Ann Arbor, MI, 1993.
4. Vincent, J. D., *Fundamentals of Infrared Detector Operation and Testing*, John Wiley & Sons, New York, 1990.
5. http://mso.anu.edu.au/observing/docs/manual/node233.html
6. Thornton, S. T., and Rex A., *Modern Physics for Scientists and Engineers*, Saunders College Publishing, Fort Worth, 1993.
7. *Space Based Infrared System SBIRS*, Space and Missile Systems Center, Los Angeles AFB.

8. Omar, M. A., *Elementary Solid State Physics*, Addison-Wesley Publishing Company, Reading, MA, 1975.

9. Larson, W. J., and Wertz, J. R., (ed.), *Space Mission Analysis and Design*, Microcosm, Inc., Torrance, CA, 1992.

10. Hovanessian, S. A., *Introduction to Sensor Systems*, Artech House, Norwood, MA, 1988.

11. Isakowitz, S. J., *International Reference Guide to Space Launch Systems*, American Institute of Aeronautics and Astronautics, Washington, DC, 1991.